Original Article

DETECTION OF *rpoB* MUTATIONS IN RIFAMPICIN-RESISTANT *MYCOBACTERIUM KANSASII*

[1]Shiomi YOSHIDA, [1]Katsuhiro SUZUKI, [1]Kazunari TSUYUGUCHI, [4]Tomotada IWAMOTO, [2]Motohisa TOMITA, [1]Masaji OKADA, [3]Mitsunori SAKATANI

Abstract [Purpose] To detect rifampicin-resistant mutations in *Mycobacterium kansasii* (*M. kansasii*).

[Methods] We examined the *M. kansasii* isolates from sputum of patients at National Hospital Organization Kinki-chuo Chest Medical Center from January 1, 2001 to November 30, 2005 using drug-susceptibility testing, and analyzed 69-bp fragment of *rpoB* gene in rifampicin-resistant strains.

[Results] Three strains from 314 isolates were determined as rifampicin resistant using drug-susceptibility testing. Those strains showed a rise in minimum inhibitory concentration (MIC), and had the mutations in *rpoB* gene. These point mutations in codons 513 and 516 were common mutations found in rifampicin-resistant clinical isolates of *M.tuberculosis*.

[Discussion] We verified the association between *rpoB* gene mutations and rifampicin resistance in *M. kansasii*.

Key words: *Mycobacterium kansasii*, Rifampicin-resistance, *rpoB* mutations, Drug-susceptibility test

[1]Clinical Research Center, [2]Department of Clinical Laboratory, [3]Department of Respiratory Medicine, National Hospital Organization Kinki-chuo Chest Medical Center, [4]Kobe Institute of Health

Correspondence to: Shiomi Yoshida, Clinical Research Center, National Hospital Organization Kinki-chuo Chest Medical Center, 1180 Nagasone-cho, Kita-ku, Sakai-shi, Osaka 591–8555 Japan. (E-mail: dustin@kch.hosp.go.jp)

Inhalational Talc Pneumoconiosis: Radiographic and CT Findings in 14 Patients

Masanori Akira[1]
Takenori Kozuka[1]
Satoru Yamamoto[2]
Mitsunori Sakatani[3]
Kenji Morinaga[4]

OBJECTIVE. The purpose of this study was to evaluate the radiographic and CT findings of inhalational talc pneumoconiosis.

CONCLUSION. Large opacities of talc pneumoconiosis progress more often than do small opacities. The CT findings of talc pneumoconiosis overlap those of silicosis and asbestosis.

Thorel [1] reported the first case of talc pneumoconiosis in 1896. Since then talc has been recognized as a cause of pneumoconiosis in miners, millers, rubber workers, and other occupational groups [2]. Talc is pure hydrous magnesium silicate with an ideal chemical composition of 63.5% SiO_2, 31.7% MgO, and 4.8% H_2O, but in practice substitutions of ions occur in the mineral lattice or the talc is contaminated by other minerals [3]. The chest radiographic manifestations of talc pneumoconiosis have been well described [4–8]. The CT features of talcosis due to IV administration of talc have been reported [9–11]. To our knowledge, however, the CT features of talc pneumoconiosis due to occupational talc exposure have not been well described [12, 13]. We present the radiographic and CT manifestations and serial changes on chest radiographs of 14 patients with pathologically proved talc pneumoconiosis.

Materials and Methods

Patients

The study included 14 patients with pathologically proved talc pneumoconiosis consecutively admitted to our hospital between 1973 and 1998. The diagnosis was based on clinical history, occupational exposure to talc dust, and histologic findings obtained at transbronchial lung biopsy ($n = 8$) or autopsy ($n = 6$). A thoracic pathologist reviewed the pathologic specimens. The pathologic findings of talc pneumoconiosis included diffuse interstitial fibrosis, ill-defined fibrotic nodules, and foreign body granulomas associated with dense accumulations of birefringent talc dust particles [1, 3]. All patients were men. The mean age was 59 years (range, 40–71 years) at initial evaluation. Mean duration of exposure to talc dust was 19 years (range, 8–35 years). Eight patients worked in a talc factory. Four patients were exposed to talc dust used in the manufacture of rubber products. One patient was exposed to talc dust used as an additive in a cosmetics factory, and one to talc dust used as an additive in a confectionery. Eleven patients ceased work after the initial evaluation. Ten patients were smokers, and four never smoked. Smokers had a smoking history ranging from 18 to 69 pack-years (mean, 36.3 pack-years).

The patients underwent follow-up chest radiography. Serial radiographs were available for all patients during a mean follow-up period of 16 years (range, 6–25 years). All patients underwent one or more CT examinations between 1988 and 2004. Chest radiographs obtained within 1 week of CT were available for all patients. After 6–25 years of follow-up, four patients had died of respiratory failure, one patient had died of myocardial infarction, and one had died of cerebral infarction. The postmortem lungs from one patient were inflated, fixed in formalin, and subjected to thin-section CT and low-kilovoltage radiography. Informed consent was provided by the patients, and the study was approved by the internal review board at the hospital.

Chest Radiographic Evaluation

Two reviewers independently interpreted the radiographs according to the 1980 International Labor Organization classification of pneumoconiosis [14]. The reviewers were a respiratory physician with a special interest in pneumoconiosis and a thoracic radiologist; both were certified by the National Institute for Occupational Safety and Health. The radiographs were interpreted in random order. Profusion of small opacities was scored with the International Labor Organization grading system on the basis of the viewer's assessment of the concentration of

Keywords: chest, high-resolution CT, lung, pneumoconiosis, radiography, talc, thin-section CT

DOI:10.2214/AJR.05.0865

Received May 23, 2005; accepted after revision August 9, 2005.

[1]Department of Radiology, Kinki-Chuo Chest Medical Center, 1180 Nagasone-cho, Sakai City, Osaka 591-8555, Japan. Address correspondence to M. Akira.

[2]Department of Pathology, Kinki-Chuo Chest Medical Center, Osaka 591-8555, Japan.

[3]Department of Internal Medicine, Kinki-Chuo Chest Medical Center, Osaka 591-8555, Japan.

[4]Department of Environmental Health, National Institute of Industrial Health, Kawasaki 214-8585, Japan.

AJR 2007; 188:326–333

0361–803X/07/1882–326

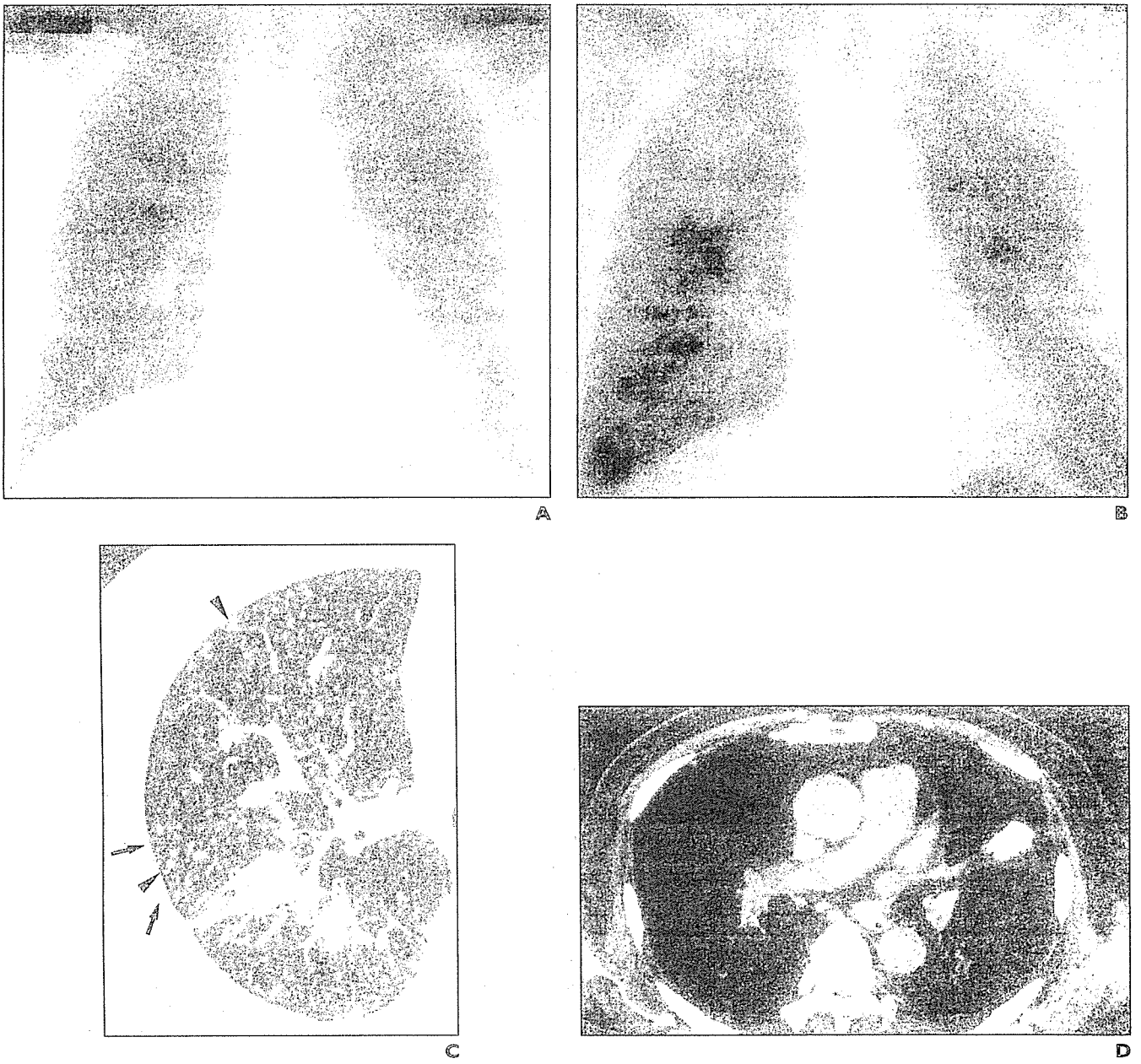

Fig. 1—61-year-old man with inhalational talc pneumoconiosis employed in talc industry for 20 years.
A, Initial chest radiograph shows fine nodular opacities diffusely distributed throughout both lungs.
B, Chest radiograph obtained at 15-year follow-up examination shows fine nodules and large opacity in upper zone of right lung and middle zone of left lung.
C, Axial supine thin-section CT scan shows well-defined (*arrowheads*) and ill-defined (*arrows*) small nodular opacities mainly distributed in centrilobular location.
D, Axial supine thin-section CT scan obtained at mediastinal settings shows large opacity and lymph nodes containing high-attenuation material.

opacities compared with standard radiographs provided by the International Labor Organization [14].

In the International Labor Organization system, profusion of small opacities is recorded on a 12-point incremental scale together with the predominant type of opacity. Category 0 includes scores 0/–, 0/0, and 0/1; category 1, scores 1/0, 1/1, and 1/2; category 2, scores 2/1, 2/2, and 2/3; and category 3, scores 3/2, 3/3, and 3/+. For small rounded opacities, the three size ranges are denoted by the letters p, q, and r: p indicates opacities with diameters up to approximately 1.5 mm; q, opacities 1.5–3 mm in diameter; and r, opacities 3–10 mm in diameter. The three size ranges of small irregular opacities are denoted by the letters s, t, and u: s indicates opacities with a width up to approximately 1.5 mm; t, opacities 1.5–3 mm in width; and u, opacities 3–10 mm in width. A large opacity is defined as an opacity exceeding 10 mm in longest dimension. The categories of large opacities are as follows: A, one large opacity up to approximately 50 mm in longest dimension or

TABLE 1: Initial and Last Chest Radiographic Findings

Patient Age (y)	Initial Radiographic Findings			Last Radiographic Findings		
	Small Opacities		Large Opacities	Small Opacities		Large Opacities
	Shape	Profusion[a]		Shape	Profusion[a]	
61	p	2/2	0	p	2/2	A
57	p/q	2/2	B	p/q	2/1	C
64	p	2/2	0	p	2/2	B
40	p	2/2	B	p	2/3	B
57	p/q	2/2	C	p/q	2/2	C
56	p/q	2/2	B	p/q	2/2	C
71	p	2/2	A	p	2/3	A
51	p	2/2	A	p	2/2	A
63	p	1/1	0	p	1/1	0
56	p	2/1	0	p	2/1	0
64	p	2/2	0	p	2/2	0
61	p	1/2	0	p	1/2	0
66	s/t	3/2	0	s/t	3/2	0
63	p	1/1	B	p	1/1	C

Note—All patients were men. p = rounded, diameter up to approximately 1.5 mm; q = rounded, diameter of 1.5–3 mm; s = irregular, width up to approximately 1.5 mm; t, irregular, width of 1.5–3 mm. 1 = slight, 2 = moderate, 3 = advanced, 0 = normal. A = A one opacity with longest dimension up to approximately 50 mm or several opacities with sum of longest dimensions not exceeding approximately 50 mm, B = one opacity with longest dimension exceeding 50 mm but not exceeding equivalent area of right upper zone or several opacities with sum of longest dimensions exceeding 50 mm but not exceeding equivalent area of right upper zone, C = one opacity exceeding equivalent area of right upper zone or several opacities that combined exceed equivalent area of right upper zone.

[a]When there is no doubt, the profusion score is 0/0, 1/1, 2/2, or 3/3. If the category above or below is considered an alternative, this category is recorded after the slash.

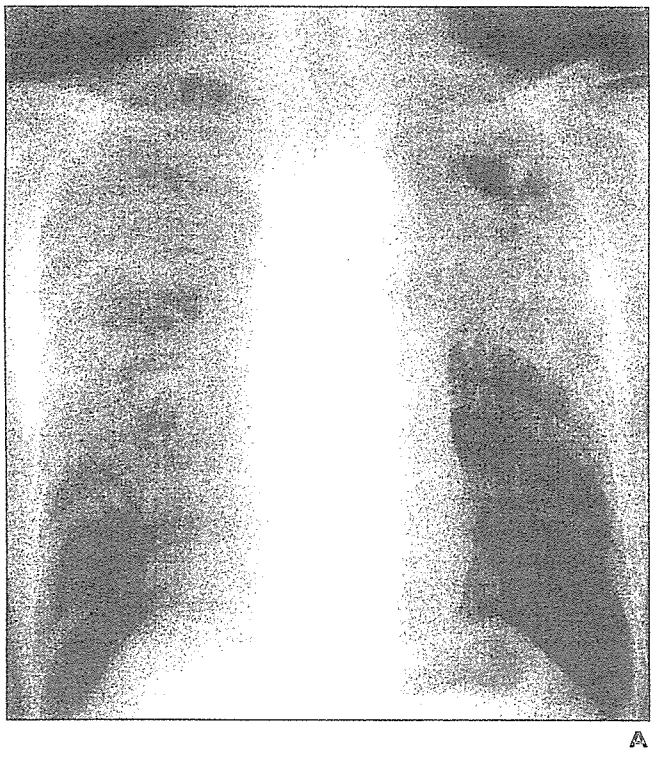

A

B

Fig. 2—57-year-old man with inhalational talc pneumoconiosis employed in talc industry for 14 years.
A, Chest radiograph shows small nodular opacities and large opacity.
B, Chest radiograph obtained at 13-year follow-up examination shows large opacities associated with bilateral superior retraction of hila.
(Fig. 2 continues on next page)

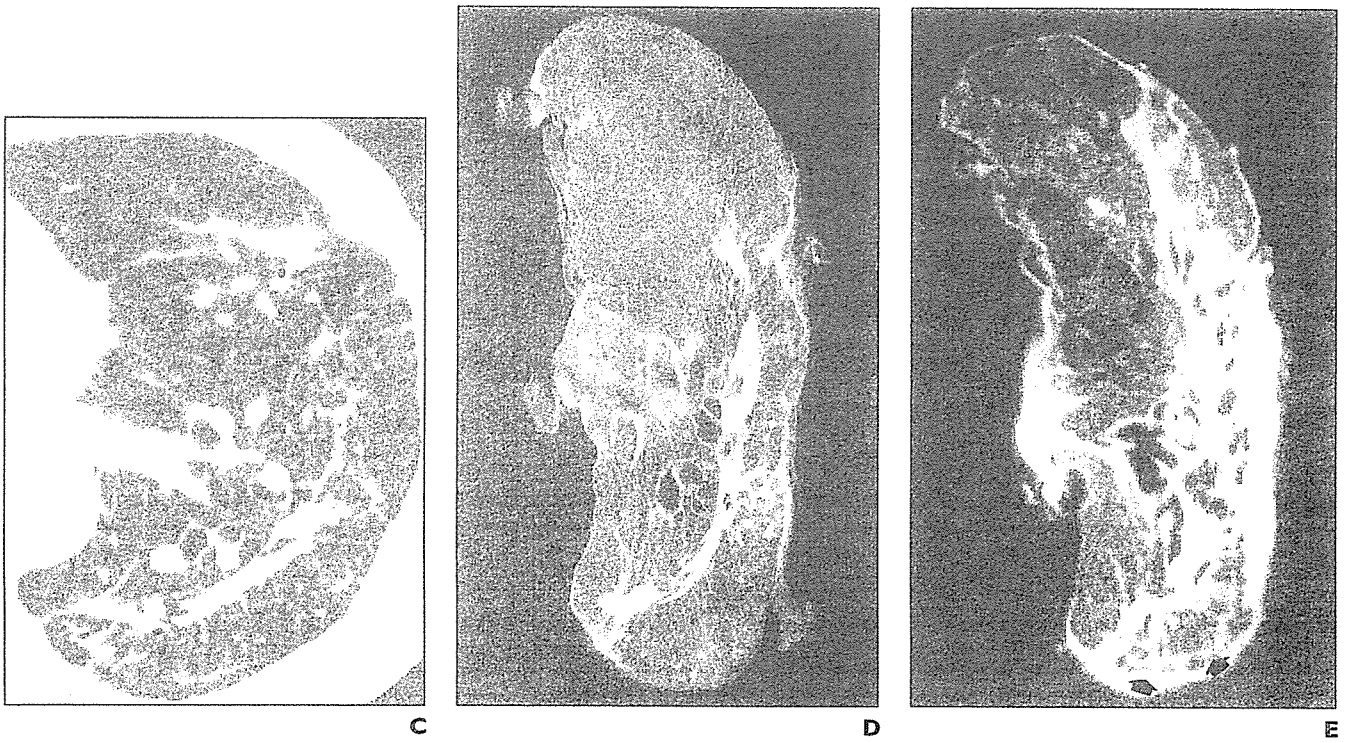

Fig. 2 (continued)—57-year-old man with inhalational talc pneumoconiosis employed in talc industry for 14 years.
C, Axial supine thin-section CT scan shows bandlike opacity parallel to pleural surface.
D, In vitro low-kilovoltage radiograph of inflated and fixed lung. Crescent-shaped large opacity and small nodular opacities are evident.
E, In vitro thin-section CT scan of inflated and fixed lung. Crescent-shaped large opacity is attached to pleural surface. Subpleural line (*arrows*) is evident.
F, Photograph of histologic section through crescentic large opacity shows diffuse fibrosis and proliferation of dust-laden macrophages and multinucleated giant cells (*arrows*). (H and E, ×4)
(Fig. 2 continues on next page)

several large opacities with the sum of longest dimensions not exceeding approximately 50 mm; B, one large opacity exceeding 50 mm in longest dimension but not exceeding the equivalent area of the right upper zone or several large opacities with the sum of longest dimensions exceeding 50 mm but not exceeding the equivalent area of the right upper zone; and C, one large opacity exceeding the equivalent area of the right upper zone or several large opacities that combined exceed the equivalent area of the right upper zone.

When the findings of the two observers did not agree, a third reviewer resolved the differences. For assessment of the sequential changes in large opacities, all radiographs for each patient were examined in side-by-side review in chronologic order by one chest radiologist.

CT Images

Thin-section CT was performed with a Quantex Plus or a LightSpeed CT unit (GE Healthcare). All CT scans were obtained at maximal inspiration with 1.5-mm collimation at 20-mm intervals. CT scans at maximal expiration were added for two patients whose inspiratory CT scans showed lobular low-attenuation areas. Scanning extended from the lung apices to below the costophrenic angles. Images were reconstructed with a high-spatial-frequency algorithm. CT scans were obtained with the patient in the supine position. The images were photographed on hard copy at lung (window width, 1,200 H; level, –700 H) and soft-tissue (window width, 300 H; level, 10 H) settings.

CT Evaluation

The CT images were reviewed independently by two chest radiologists unaware of the clinical and radiographic data. The final decisions on CT findings were reached by consensus. The reviewers evaluated the scans for the presence and distribution of ground-glass opacity, septal lines, subpleural lines, small rounded opacities, centrilobular

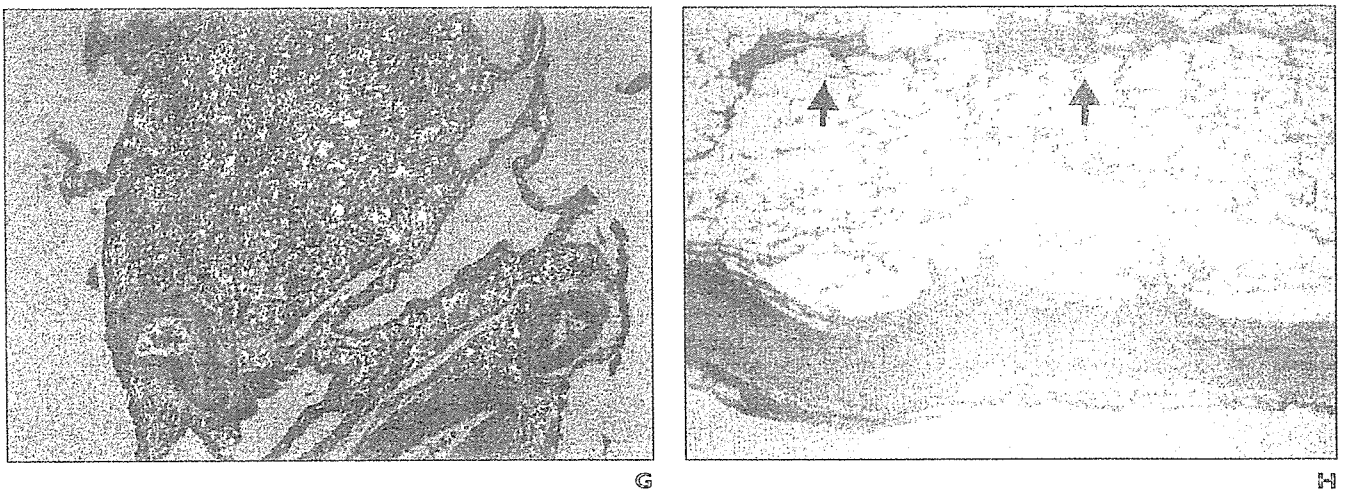

G H

Fig. 2 (continued)—57-year-old man with inhalational talc pneumoconiosis employed in talc industry for 14 years.
G, Photomicrograph of biopsy specimen examined under polarized light shows fibrosis contains large accumulations of strongly birefringent dust particles.
H, Histologic section from area of subpleural line shows peribronchiolar fibrosis joined by collapse and fibrosis of alveoli along thickened pleura (*arrows*). (H and E, ×1.6)

nodules, small irregular opacities, large opacities, traction bronchiectasis, honeycombing, lobular low-attenuation areas, and emphysema [15, 16].

Areas of ground-glass attenuation were defined as areas of hazy high attenuation that did not obscure the underlying vascular markings. Septal thickening was defined as short lines in perpendicular contact with the pleural surface or a pattern of multiple polygonal lines representing thickened interlobular septa. Subpleural lines were defined as linear areas of increased attenuation within 1 cm of the pleura and parallel to the inner chest wall. Small rounded opacities were defined as nodules less than 10 mm in diameter. Centrilobular nodules were recorded if nodules were identified around peripheral pulmonary arterial branches or 3–5 mm away from the pleura, interlobular septa, or pulmonary veins. Small irregular opacities were defined as intersecting lines that formed a fine or coarse network. Large opacity was defined as an opacity having a diameter exceeding 10 mm. Traction bronchiectasis was defined as bronchial dilatation within areas of a parenchymal abnormality. Honeycombing was defined as an accumulation of cystic spaces with thickened walls. Lobular low-attenuation areas were defined as areas of decreased attenuation with a lobular or multilobular distribution adjacent to areas of high attenuation. Emphysema was characterized by areas of decreased attenuation, disruption of the vascular pattern, and absence of a well-defined wall.

For craniocaudal distribution, the upper lung zone was defined as the region above the tracheal carina; the middle zone as the region between the carina and inferior pulmonary veins; and the lower zone as the region below the inferior pulmonary veins. Calcified or noncalcified pleural plaques and lymph node enlargement with the short axis exceeding 1 cm were also recorded.

Results

Chest Radiographic Findings

The main abnormality found on initial chest radiographs was small rounded opacities of the p type (Fig. 1A). All zones usually were affected. In one patient, the opacities had upper lung zone predominance, and in another middle lung zone predominance. Small irregular opacities of the s and t types predominated in the lower lung zones in one patient. The profusion and type of small opacities are presented in Table 1. Large opacities greater than 1 cm in diameter were found in seven patients on initial chest radiographs (Fig. 2A). The large opacities were distributed in the upper lung zones in two patients, in the middle lung zones in one patient, in the upper and middle lung zones in three patients, and in all zones in one patient.

Follow-up examinations of two of the 14 patients showed the small opacities had progressed. Profusion had changed from 2/2 to 2/3. In another patient, profusion of small opacities decreased from 2/2 to 2/1, but that of large opacities increased. The other 11 patients had no change during the follow-up period. The size and number of large opacities had increased by the follow-up examination in all seven patients (Figs. 1B and 2B). At the follow-up examinations of another two patients, large opacities were present in the upper, middle, and lower zones. Progression of large opacities was found to be a difference of one grade in four patients (from 0 to A in one and from B to C in three) and a difference of two grades in one patient (from 0 to B). In another four patients, progression was within the same grade (from A to A in two, B to B in one, and C to C in one). In these four patients, progression of large opacities was found at side-by-side review of the radiographs in chronologic order. Lymph node enlargement was found in two patients. Pleural plaques were found in no patients.

Thin-Section CT Findings

The thin-section CT findings for the 14 patients are presented in Table 2. The main CT finding in 12 of 14 patients was diffusely distributed centrilobular nodules 1–2 mm in diameter. In one patient, the centrilobular nodules had upper lung predominance; in another patient, middle lung predominance; and in 10 patients, no zonal predominance. A few well-defined discrete nodules were found in these 12 patients, mingled with centrilobular nodules in all zones (Fig. 1C). Well-defined nodules ranged from 2 to 4 mm in diameter and were in a centrilobular or subpleural location. In one patient, CT scans showed small irregular opacities and honeycombing in the lower lung zones and diffusely distributed centrilobular nodules in all zones. In another patient, CT showed large opacities in the upper and middle lung zones and a few well-defined small rounded opacities distributed in all lung zones.

Large opacities greater than 1 cm in diameter were found in nine patients. The large opacities involved all lung zones in four patients, the upper zones in one patient, the upper and middle zones in three patients, and the

TABLE 2: Prevalence of Thin-Section CT and Radiographic Findings in 14 Patients

Finding	CT	Radiography
Large opacities	9	9
Small rounded opacities	14	14
Small regular opacities	1	1
Centrilobular nodules	13	NA
Septal lines	10	2
Subpleural lines	9	NA
Ground-glass opacity	8	0
Traction bronchiectasis	4	NA
Honeycombing	1	1
Emphysema	5	3
Lobular low-attenuation area	5	NA
Pleural plaque	7	0
Noncalcified	3	
Calcified	4	
Lymph node enlargement	8	2

Note—NA = not applicable to radiography.

Fig. 3—66-year-old man with inhalational talc pneumoconiosis. Axial supine thin-section CT scan shows subpleural line.

middle and lower zones in one patient. The large opacities were irregular, round, or crescent-shaped (Fig. 2C). Most large opacities were totally of high attenuation (Fig. 1D).

The other frequent findings included septal lines ($n = 10$), subpleural lines ($n = 9$) (Fig. 3), and ground-glass opacity ($n = 8$). Emphysema was found in five patients, and all five of these patients were smokers. Lobular low-attenuation areas were seen in five patients, and two of these five patients were nonsmokers. On expiratory CT scans of two patients, air trapping and low-attenuation areas were delineated more clearly but did not newly appear elsewhere, and additional areas of low attenuation were not identified. Septal lines and emphysema were present in all lung zones. Subpleural lines, ground-glass opacity, and lobular low-attenuation areas were present in a random distribution.

Slight lymph node enlargement of increased attenuation was visible in eight patients (Fig. 1D). Noncalcified pleural plaques were seen in three patients and calcified pleural plaques in four patients. Lymph node enlargement in six of the eight patients and pleural plaques were not found on chest radiographs (Table 2).

There was good agreement between observers. In two cases there was disagreement about chest radiographs and in one case about CT scans.

Radiologic–Pathologic Correlation

The postmortem low-kilovoltage radiographs and thin-section CT scans of one patient showed a crescent-shaped large opacity, subpleural lines, and small nodules (Figs. 2D and 2E). The crescent-shaped large opacity corresponded histologically to diffuse fibrosis with proliferation of dust-laden macrophages and multinucleated giant cells (Fig. 2F). Microscopic evaluation with polarized light revealed dense accumulations of birefringent dust particles in fibrosis (Fig. 2G). The subpleural lines corresponded histologically to peribronchiolar fibrosis joined by collapse and fibrosis of the alveoli along the inner chest wall (Fig. 2H).

Fig. 4—77-year-old man with inhalational talc pneumoconiosis. Histopathologic photograph shows nodular fibrosis (*arrows*) adjacent to vessels or bronchi. (H and E, ×1.25)

In six autopsy cases, the lungs exhibited varying degrees of fibrosis. Nodular fibrosis was adjacent to the vessels or bronchi (Fig. 4). Dense accumulations of birefringent dust particles were found in fibrosis and lymph nodes, but calcification was not found in fibrosis or lymph nodes. Pleural plaques were found at histopathologic examination in three of six autopsy cases. In these three cases, the premortem CT scans showed pleural plaques.

Discussion

Three forms of talc pneumoconiosis by inhalation have been described in the literature: talc asbestosis, talc silicosis, and talcosis. Talc asbestosis is produced by inhalation of talc with asbestiform fibers. The findings of talc silicosis caused by talc mined with high-silica-content mineral are identical to those of silicosis. Talc free of silica and asbestiform minerals may be fibrogenic [3, 4, 8, 17].

In our cases, the predominant radiographic abnormalities were small nodular opacities affecting all lung zones. Small irregular opacities were rare. Although progression of small rounded opacities was rare during long-term follow-up, most large opacities progressed. Slight pleural plaques and lymph node enlargement not found on chest radiographs were identified on thin-section CT scans.

As in patients with silicosis, in our pneumoconiosis patients, small rounded opacities, septal lines, large opacities, and lymph node enlargement were predominant findings on CT. The characteristic radiologic abnormality in silicosis is small, well-circumscribed nodules usually 2–5 mm in diameter and mainly involving the upper and posterior lung zones [12, 18]. In our patients, however, centrilobu-

TABLE 3: Comparative CT Findings in Talc Pneumoconiosis, Asbestosis, and Silicosis

Finding	Talc Pneumoconiosis	Asbestosis	Silicosis
Small rounded opacities	Present	Present	Absent
Small irregular opacities	Present	Absent	Present
Septal lines	Present	Present	Present
Subpleural lines	Present	Absent	Present
Large opacities	Present	Present	Absent
Lymph node enlargement	Present	Present	Absent
Lobular low-attenuation area	Present	Absent	Present
Pleural plaque	Present	Absent	Present
Predominant distribution	Diffuse	Upper	Lower

Note—Data are based on CT findings in the present study and summary of CT findings in asbestosis and silicosis adapted from [12, 18, 19].

lar nodules were the prominent finding, and the distribution was diffuse. In silicosis, large opacities usually involve the upper lung zones, and various types of calcification of large opacities are found, mostly punctate rather than linear or massive. In our patients, large opacities were distributed in all lung zones, and large opacities were of high density. Unlike the findings in patients with silicosis, pleural plaques were seen in our patients (Table 3). One of our patients had the CT findings of asbestosis: diffuse linear interstitial pattern predominantly distributed in the lower zones of the lungs [12, 19]. Diffusely distributed centrilobular nodules unlike the findings of asbestosis were found on that patient's CT scans.

Subpleural curvilinear lines are defined as linear areas of increased attenuation within 1 cm of the pleura and parallel to the inner chest wall. The pathologic correlate of subpleural lines represents peribronchiolar fibrotic thickening combined with flattening and collapse of the alveoli due to fibrosis in asbestosis [20, 21]. Subpleural curvilinear lines are considered to be caused by other pathologic processes. This finding corresponds to conditions such as platelike atelectasis in the corticomedullary junction of the lung [22], interstitial edema from pulmonary congestion [23], and subpleural lymphatic network after lymphography [24].

The main CT findings in three patients with inhalational pulmonary talcosis described by Marchiori and associates [13] were small centrilobular and subpleural nodules associated with conglomerated masses containing foci of high attenuation. Our findings were similar to those of Marchiori et al. In our study, centrilobular nodules histopathologically corresponded to nodular fibrosis and deposition of talc particles adjacent to the vessels or bronchi. Our study revealed that increased CT densities of lymph nodes and large opacities were caused by large numbers of talc particles.

The radiographic findings of IV administration of talc include large, irregular, nodular densities or consolidations in the upper parts of the middle fields of the lungs that may rapidly progress into large masses or massive consolidations. Widespread irregular nodules also occur [9–11]. The CT findings in patients with pulmonary talcosis resulting from chronic IV drug abuse include widespread ground-glass attenuation, a diffuse fine nodular pattern, and a combination of nodules and lower lobe panacinar emphysema. Confluent perihilar masses with areas of high attenuation are also seen [9–11]. The CT findings in our patients resembled those of pulmonary talcosis due to IV administration. A diffuse fine nodular pattern and large opacities containing high-attenuation material are seen in both IV administration and inhalation. Although lobular low-attenuation areas were seen, lower lobe panacinar emphysema was not seen in our patients. To our knowledge, slight lymph node enlargement with high-attenuation material has not been reported in talcosis by IV administration. Talcosis from IV administration of talc can be differentiated from the inhalation of talc on the basis of histologic findings and size of the talc particles. The mean particle diameter is far greater in IV-administrated talc, usually exceeding 10 μm compared with 4 μm for inhaled talc [25].

We did not analyze the nature of the mineral exposure in our patients, so it is not clear whether our findings were caused by contaminant fibers. The composition of commercially available talc is quite variable from region to region and from industry to industry. Pleural plaques are seen in workers exposed to talc contaminated with asbestos and talc free of asbestos [26]. Our study had limitations. It was retrospective, and the preliminary conclusions were based on findings in a relatively small number of patients.

In summary, serial chest radiography showed that in talc pneumoconiosis, large opacities progressed more often than small rounded opacities. CT scans depicted pleural plaques and lymph node enlargement with high-attenuation material not identified on chest radiography. The distribution of small rounded opacities was diffuse, whereas large opacities were present in all lung zones. Unlike silicosis, in talc pneumoconiosis there was no predilection for upper lung zones. Pleural plaques and subpleural lines and small rounded opacities were evident. CT showed high-attenuation material in large opacities and lymph node enlargement caused by large numbers of talc particles. The CT findings of talc pneumoconiosis are not specific and can occur in asbestosis and silicosis. Although the combination of these findings is seen in patients with mixed dust exposure, talc pneumoconiosis should be considered in patients with diffusely distributed centrilobular nodules, dense large opacities, dense lymph nodes, and pleural plaques.

References

1. Thorel C. Talc lung: a contribution to the pathological anatomy of pneumoconiosis. *Beitr Pathol Anat Allgem Pathol* 1896; 20:85–101
2. Vallyathan NV, Craighead JE. Pulmonary pathology in workers exposed to nonasbestiform talc. *Hum Pathol* 1981; 12:28–35
3. Gibbs AE, Pooley FD, Griffiths DM, Mitha R, Craighead JE, Ruttner JR. Talc pneumoconiosis: a pathologic and mineralogic study. *Hum Pathol* 1992; 23:1344–1354
4. Feigin DS. Talc: understanding its manifestations in the chest. *AJR* 1986; 146:295–301
5. Leophonte P, Didier A. French talc pneumoconiosis. In: Bignon J, ed., *Health-related effects of phyllosilicates*. Berlin, Germany: Springer Verlag, 1990:203–209
6. Porro FW, Patton JR, Hobbs AA. Pneumoconiosis in the talc industry. *AJR* 1942; 47:507–524
7. Kleinfeld M, Messite J, Tabershaw IR. Talc pneumoconiosis. *AMA Arch Ind Health* 1955; 12:66–72
8. Feigin DS. Misconceptions regarding the pathogenicity of silicas and silicates. *J Thorac Imaging*

1989; 4:68–80

9. Padley SP, Adler BD, Staples CA, Miller RR, Müller NL. Pulmonary talcosis: CT findings in three cases. *Radiology* 1993; 186:125–127
10. Ward S, Heyneman LE, Reittner P, Kazerooni EA, Godwin JD, Müller NL. Talcosis associated with IV abuse of oral medications: CT findings. *AJR* 2000; 174:789–793
11. Stern EJ, Frank MS, Schutz JF, Glenny RW, Schmidt RA, Godwin JD. Panlobular pulmonary emphysema caused by IV injection of methylphenidate (Ritalin): findings on chest radiographs and CT scans. *AJR* 1994; 162:555–560
12. Akira M. High-resolution CT in the evaluation of occupational and environmental disease. *Radiol Clin North Am* 2002; 40:43–59
13. Marchiori E, Souza AS Jr, Müller NL. Inhalational pulmonary talcosis: high-resolution CT findings in 3 patients. *J Thorac Imaging* 2004; 19:41–44
14. *Guidelines for the use of ILO international classification of radiographs of pneumoconiosis,* rev ed. Occupational Safety and Health Series no. 22. Geneva, Switzerland: International Labor Organization, 1980
15. Austin JH, Müller NL, Friedman PJ, et al. Glossary of terms for CT of the lungs: recommendations of the nomenclature committee of the Fleischner Society. *Radiology* 1996; 200:327–331
16. Im JG, Kim SH, Chung MJ, Koo JM, Han MC. Lobular low attenuation of the lung parenchyma on CT: evaluation of forty-eight patients. *J Comput Assist Tomogr* 1996; 20:756–762
17. Lockey JE. Nonasbestos fibrous minerals. *Clin Chest Med* 1981; 2:203–218
18. Kim KI, Kim CW, Lee MK, et al. Imaging of occupational lung disease. *RadioGraphics* 2001; 21:1371–1391
19. Aberle DR, Gamsu G, Ray CS, Feuerstein IM. Asbestos-related pleural and parenchymal fibrosis: detection with thin-section CT. *Radiology* 1988; 166:729–734
20. Akira M, Yokoyama K, Yamamoto S, et al. Early asbestosis: evaluation with high-resolution CT. *Radiology* 1991; 178:409–416
21. Yoshimura H, Hatakeyama M, Otsuji H, et al. Pulmonary asbestosis: CT study of subpleural curvilinear shadow. *Radiology* 1986; 158:653–658
22. Kubota H, Hosoya T, Kato M, Uchimura F, Itagaki T, Yamaguchi K. Plate-like atelectasis at the corticomedullary junction of the lung: CT observation and hypothesis. *Radiat Med* 1983; 1:305–310
23. Arai K, Takashima T, Matsui O, Kadoya M, Kamimura R. Transient subpleural curvilinear shadow caused by pulmonary congestion. *J Comput Assist Tomogr* 1990; 14:87–88
24. Pilate I, Marcelis S, Timmerman H, Beeckman P, Osteaux MJ. Pulmonary asbestosis: CT study of subpleural curvilinear shadow. (letter) *Radiology* 1987; 164:584
25. Abraham JL, Brambilla C. Particle size for differentiation between inhalation and injection pulmonary talcosis. *Environ Res* 1980; 21:94–96
26. Wegman DH, Peters JM, Boundy MG, Smith TJ. Evaluation of respiratory effects in miners and millers exposed to talc free of asbestos and silica. *Br J Ind Med* 1982; 39:233–238

*Mycobacterium kansasii*株における分子疫学的解明

[1]吉田志緒美 [1]鈴木 克洋 [1]露口 一成 [3]岩本 朋忠
[1]岡田 全司 [2]坂谷 光則

要旨：〔目的〕*M. kansasii*株に対する各種遺伝子型別法を用いた分子疫学的解明。〔対象と方法〕2002年6月1日から2005年8月31日の期間，近畿中央胸部疾患センターにおいて臨床検体から分離，同定された*M. kansasii* 174株を対象として，*hsp* 65-PRA，ITSシークエンス，PFGE，IS*1652*-RFLPならびにMPTR-RFLPを行った。また*hsp*65-PRAとITSシークエンスの結果に乖離があった株に対しては*hsp*65シークエンスを行った。〔結果〕*hsp*65-PRAの結果，174株中Ⅰ型が170株（97.7%）を占め，Ⅱ型は2株，Ⅱb型は1株，Ⅵ型は1株に認められた。ITSシークエンスではⅠ型，Ⅱ型，Ⅵ型の*M. kansasii*が*hsp*65-PRAと同じ型を認め，Ⅱb型はITS sequevar typeⅡと判定された。IS*1652*-RFLPとMPTR-RFLPの結果，Ⅰ型の170株は同一のバンドパターンを示し，Ⅰ型以外の型（Ⅱ型，Ⅱb型，Ⅵ型）を示した4株に多型性が認められた。PFGEでは，159株（91.4%）がクラスターを形成し，残り15株に多型性を認めた。〔結論〕今回各種遺伝子型別法を用いて遺伝子型別を試みた結果，世界的に蔓延しているⅠ型が当センター周辺地域においても高い割合で分布している状況が認められ，Ⅰ型の高いクローナリティーが示唆された。またPFGEによりⅠ型に亜分類が存在する可能性が考えられた。

キーワーズ：*Mycobacterium kansasii*，*hsp*65-PRA，16S-23S ITSシークエンス，PFGE，RFLP

はじめに

Mycobacterium kansasii（*M. kansasii*）は非結核性抗酸菌（nontuberculous mycobacteria，NTM）のⅠ群菌に分類される遅発育の光発色菌である。わが国ではNTM症の原因菌の約25%を占め，*Mycobacterium avium* complex（MAC）の次に多く症例報告されている菌種である[1]。またヒトに対する強い起病性をもち，主にヒトの肺結核類似症を引き起こす。現在*M. kansasii*はDNAプローブを用いたハイブリダイゼイション[2)3)]やシークエンス[4)]，制限酵素（restriction enzyme）処理によるDNA断片の多型解析[5)]などの解析手法を用いてⅠ～Ⅶの遺伝子型に分類されているが[6)]，各種遺伝子型別法を同時に用いた詳細な解析の報告は少ない[7)]。今回われわれは，当センターにおいて分離，同定された*M. kansasii*株を対象として，heat shock protein（*hsp*）65-polymerase chain reaction（PCR）-restriction analysis（PRA）による遺伝子型別，16S-23S internal transcribed spacer（ITS）シークエンス，pulsed-field gel electrophoresis（PFGE）による高分子DNA解析，IS*1652*ならびにmajor polymorphic tandem repeat（MPTR）のDNAプローブを用いたrestriction fragment length polymorphism（RFLP）を用い，同菌の感染状況の解明を試みた。

方　法

〔対象〕

2002年6月1日から2005年8月31日の期間，独立行政法人国立病院機構近畿中央胸部疾患センターにおいて，臨床検体から分離，同定された*M. kansasii* 174株。すべての菌株の同定は，アキュプローブ マイコバクテリウム カンサシ研究用（極東製薬）で行った。今回これらの菌由来患者174名は結核病学会の診断基準[8)]により*M. kansasii*症と診断され，HIV感染は認められなかった。

*hsp*65-PRA

Telentiらの方法[9)]に準じて行った。小川培地発育菌か

[1]独立行政法人国立病院機構近畿中央胸部疾患センター臨床研究センター，[2]内科，[3]神戸市環境保健研究所

連絡先：吉田志緒美，独立行政法人国立病院機構近畿中央胸部疾患センター臨床研究センター，〒591-8555 大阪府堺市北区長曽根町1180（E-mail: dustin@kch.hosp.go.jp）
(Received 3 Aug. 2006/Accepted 18 Oct. 2006)

ら白金耳で径2～3 mmのコロニー2個分の菌量を採取し，1.5 mlマイクロチューブに分注したインスタジーンDNA精製マトリックス（BIO-RAD）200 μlに懸濁した。56℃，15～30分処理後10秒間vortexし，正確に100℃，8分間処理した後直ちに氷水中に急冷した。10秒間vortexし，12000 rpm，3分遠心した上清をPCRに用いた。PCR増幅のために，次のプライマーを使用した；Tb11 [5'-ACC AAC GAT GGT GTG TCC AT-3'] とTb12 [5'-CTT GTC GAA CCG CAT ACC CT-3']。PCR条件は95℃ 1分の熱変性の後，96℃ 40秒，60℃ 50秒，72℃ 1分を45サイクル行い，最後に72℃ 7分間伸張した。得られたPCR増幅産物の*Bst*EⅡ切断断片長（60℃，60分処理）および*Hae*Ⅲ切断断片長（37℃，60分）を制限酵素失活処理後マイクロキャピラリー電気泳動装置Cosmo eye SV1201（カイノス）を用いて解析した。

ITSシークエンス

ITSシークエンスはRichterらの方法[10]に準じて行った。ITS 1 [5'-GAT TGG GAC GAA GTC GTA AC-3'] とITS 2 [5'-AGC CTC CCA CGT CCT TCA TC-3'] を用いてITS全長を含む領域のPCR増幅産物を得た。PCR条件は95℃ 9分の熱変性の後，94℃ 45秒，55℃ 60秒，72℃ 90秒を30サイクル行い，最後に72℃ 7分間伸張した。BigDye Terminator v1.1 Cycle sequencing Kit（ABI）を用いて，ITS全長の塩基配列を決定した。

PFGE

Iinumaらの方法[11]に準じて行った。

1. 菌液調整，サンプルブロックの作成

ミドルブルック7H9培地（BBL）を用いて，*M. kansasii*株を37℃，7～14日間培養し，McFarland No. 2～3の濁度に調整した後，D-cycloserineを1 mg/ml加え，12～18時間培養を続けた。次いで培養液を遠心し，TS溶液［50 mM Tris HCl（pH8.0），0.5 M Sucrose/100 ml］に再浮遊して，－40℃で凍結，その後直ちに氷水中で融解した（Freeze and Sawing）。菌液70 μlに対し，1.5%低融点アガロース（BIO-RAD）70 μlを混合し，その混合液120 μlを速やかにPFGE用インサートモールドに挿入し固相化した。

2. 溶菌，除タンパク，制限酵素処理

リゾチーム4 mg/ml加Lysis溶液500 μlにサンプルブロックを入れ，溶菌処理（37℃，18時間）後，Proteinase K（1.0 mg/ml）加ES溶液900 μlにゲルを移し変えて除タンパク処理（50℃，18時間）を行った。次いでProteinase Kの不活化処理のため，Pefabloc 1.5 mM/ml加TE溶液を500 μl入れたチューブに，サンプルブロックを0.5 mm幅にスライスしたサンプルプラグを入れ，室温で2時間振盪した。TE溶液で30分，3回の洗浄処理を行い，2回のpre-incubationの後，*Dra*Ⅰ（100U）による制限酵素処理（37℃，18時間）を行った。

3. 電気泳動

0.5%TBE溶液に溶かした1%アガロースゲルにサンプルプラグを挿入した。14℃に冷却した0.5%TBE溶液2000 mlを泳動槽に循環させ，PFGE泳動装置CHEF DR Ⅲ（BIO-RAD）を用いて19.5時間の電気泳動を行った。

4. 染色，撮影，画像処理，系統樹作成

ゲルをethidium bromide（EtBr）溶液に30分振盪して染色を行い，撮影した。Phoretix 1D Pro（Nonlinear Dynamics社）を用いてゲルイメージ解析処理を行い，Phoretix 1D Database（Nonlinear Dynamics社）を使用してデータベース化し系統樹を作成した。

IS*1652*-RFLP

IS*1652*配列は*M. kansasii*に特異的な947 bpの長さを保有した配列であるが，DNAプローブのpMK1-9[12]に陰性の*M. kansasii*にのみ認めるとされている[2]。今回われわれはYangらの方法[12]に準じて行った。IS*1652*プローブはIS 1 [5'-TCC TCC GTG CGC GCT GGA GC-3'] とIS 2 [5'-CGG ACC TGC CCA TCA GCG TC-3'] を用いて作成し，各種制限酵素*Alu*Ⅰ，*Eco*RⅠ，*Pvu*Ⅱ，*Sma*Ⅰについてそれぞれのパターンの比較から多型性の検討を行った。

MPTR-RFLP

10 bpの繰り返し配列で，5 bpの間隔をもつMPTR配列は*M. kansasii*以外に結核菌群，*M. gordonae*，*M. asiaticum*，*M. gastri*，*M. szulgai*にも存在する[3][13]。結核菌の染色体上には100以上のコピー数をもつ多型性を示すが，*M. kansasii*に対しては高い分離能が認められている[13]。今回Hermansらの方法[13]に準じて，IS*1652*-RFLPと同様，制限酵素*Bst*EⅡ，*Sma*Ⅰを用いて多型性の検討を行った。

結　果

*hsp*65-PRA，ITSシークエンス

M. kansasii 174株中170株（97.7%）が*hsp*65-PRA，ITSシークエンスでともにⅠ型と認められた。残り4株のうち，2株は両手法でⅡ型に，1株はⅥ型と認められたが，*hsp*65-PRAパターンによる型別とITSシークエンスによる型別での食い違いを示す株が1株認められた（Table 1）。この株のPRAパターンはIwamoto and Saito[14]の定義したⅡb型のパターンを示し，ITSシークエンスはⅡ型の配列であった。Ⅱb型のPRAパターンを示した株については，*hsp*65 geneのPCR産物のシークエンスを決定し，Iwamoto and Saito[14]の報告したatypical type Ⅱと一致することを確認した。

PFGE

PFGEにより*M. kansasii* 174株は，バンドパターンの

類似した大きなグループを形成する159株とユニークなパターンを示す15株に大別された。159株は *hsp*65$_3$PRAおよびITSシークエンスですべてⅠ型に型別された。一方，ユニークなパターンの15株にはⅡ型，Ⅱb型，Ⅵ型を示した4株とⅠ型の11株が含まれていた。そこで今回のPFGE結果をPFGE電気泳動パターンの評価基準[15]に基づいて，A，B，Cの3つに分類した。グループAはバンドの変化がない同一クローナリティーと2～3バンドの違いをもつ株からなり，*hsp*65 PRAおよびITSシークエンスでⅠ型に型別された170株のうちの159株（91.4%）が分類された。グループBは4～6バンドの違いをもつ株からなり，Ⅰ型2株とⅥ型1株が分類された。グループCは7バンド以上の違いを認める株からなり，Ⅰ型9株とⅡ型2株およびⅡb型1株が分類された（Fig. 1）。

IS*1652*-RFLPならびにMPTR-RFLP

IS*1652*-RFLPではⅠ型とⅠ型以外の4株（Ⅱ型，Ⅱb型，Ⅵ型）間で多型性を示したが，Ⅰ型の170株はすべて共通したバンドパターンを示し，多型性は認められなかった。

MPTR-RFLPでも同様に，タイプ間では多型性を示したが，Ⅰ型は多型性を認めなかった（Fig. 2）。また異なる制限酵素処理による多型性分類の比較では，いずれのRFLPにおいても変化は認められなかった。

Table 1 Distribution of *Mycobacterium kansasii* isolates according to subtype in NHO Kinki-chuo Chest Medical Center (n=174)

Type	*hsp*65-PRA	Sequencing	RFLP		Subtypes by PFGE		
		ITS	IS*1652*	MPTR	A Pattern	B Pattern	C Pattern
Ⅰ	170	170	170	170	159	2	9
Ⅱ	2	3	3	3	0	0	2
Ⅱb	1*	0	0	0	0	0	1*
Ⅵ	1	1	1	1	0	1	0
Total	174	174	174	174	159	3	12

*Atypical type Ⅱ by *hsp*65 sequence

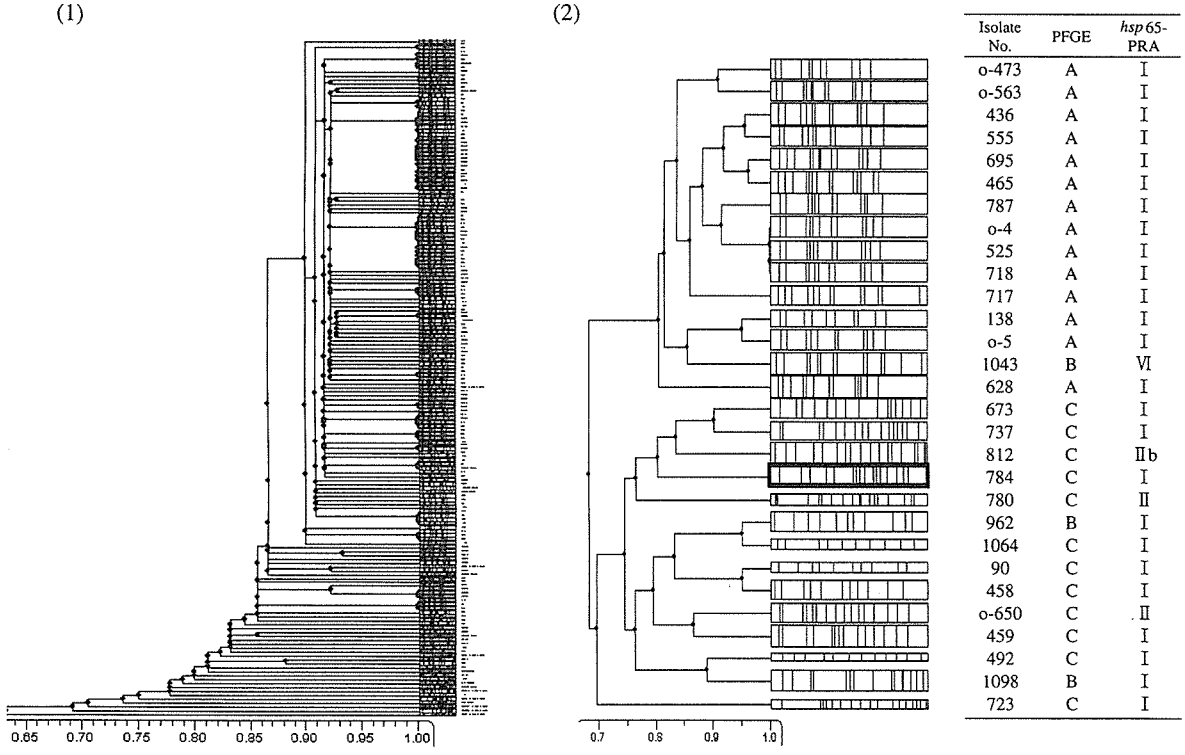

Fig. 1 Phylogenetic tree for single linkage of 174 *Mycobacterium kansasii* isolates (1) and polymorphic analysis of isolates consist of the representative pattern A, and all patterns of B and C (2) by PFGE. The pattern A showed the indistinguishable common pattern, and the pattern B and C showed polymorphous pattern by PFGE.

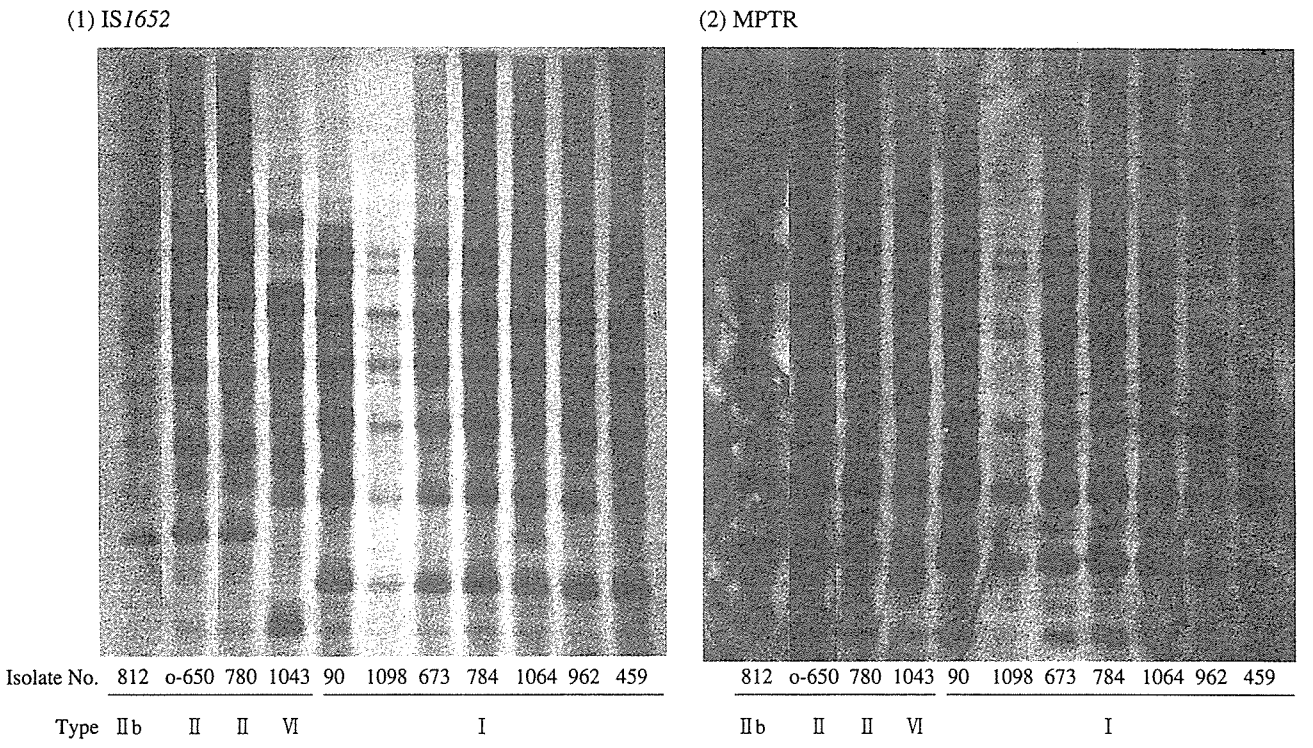

Fig. 2 RFLP analysis of IS*1652* and major polymorphic tandem repeat (MPTR) in relation to the *Mycobacterium kansasii* genotype, according *hsp* 65-PRA.

考　察

近年，分子遺伝学の発展によって，NTMの分子疫学解析に各種遺伝子型別法を応用した多くの疫学的解明の研究が進み，*M. kansasii*においてもいくつかの分子疫学的解析がなされている[6)7)14)16)]。先人の報告から*M. kansasii*が世界的に分布している状況がうかがえるが，国あるいは地域に発症頻度の分布差が見受けられる。英国ウェールズ地方では最も多いNTMであり[17)]，チェコのKarvina地方[18)]や南アフリカの鉱山[19)]でも多数報告されているが，オーストラリアではあまり分離されていない[20)]。わが国[1)]および米国[21)]ではMACに次いで多く分離されているが，米国内でも地理的に中南部に多い傾向があり[22)23)]，サンフランシスコの統計では5年間で269名の*M. kansasii*症の患者が報告されている[24)]。わが国においても症例数の増加に伴い全国的な広がりは見せているが，米国同様に流行の地域性が見られ，特に近畿圏地域は他の地域に比べて最も多い[14)]。しかも近畿圏内に位置する当センターでは年間60から70例の新規*M. kansasii*症患者が受診している。そこで感染経路の推測ならびに疫学的解明に有用な遺伝子型別解析を同菌株に対して実施することは治療戦略を図るうえでも非常に重要である。

同菌に対する代表的な解析法のひとつである*hsp* 65-PRAはTelentiら[9)]が開発したPCR-based *hsp* 65 gene内の制限酵素切断部位の多様性からNTMを分別するPCR-restriction analysis (PRA)である。Picardeauら(フランス)[7)]は*M. kansasii*の臨床分離菌39株と水道水からの分離菌24株を対象として*hsp* 65-PRAを行い，Ⅰ型～Ⅴ型の5つのタイプに分類した。また臨床分離菌191株を対象としたTaillardら(スイス)[6)]はさらにⅦ型までの7つのタイプに分類している。Picardeauら[7)]の結果ではⅠ型は39.7%，Ⅱ型は31.7%と同程度の割合を示し，Taillardら[6)]によるとⅠ型は67%，Ⅱ型は21%を占めていた。一方Chimaraら[16)]が臨床分離菌184株について検討したサンパウロでの報告では182株(98.9%)がⅠ型と認められ，Iwamoto and Saito[14)]のわが国での報告においても，臨床分離菌198株中184株(92.9%)がⅠ型に分類されている。今回われわれの検討ではⅠ型が高い割合(97.7%)で認められた。

そこで今回の解析を含めたⅠ型が多数を占めた報告[14)16)]と，Picardeauら[7)]やAlcaideら[4)]のⅡ型が比較的多い欧米の報告との間に違いが表れる理由について考察してみると，まず対象とするサンプリングの違いが考えられる。Ⅰ型が多数認められた報告[14)16)]は臨床検体のみを対象としており，一方環境由来検体を含めた場合[4)7)]にはⅡ型が多く認められている。また*M. kansasii*は自然界からの分離は稀で，同一地域の水道水から繰り返し分離される

と報告されている[21]。したがって，諸国間で異なる地理的環境の影響下におけるサンプリングの違いから，*M. kansasii* の感染状況の相違が生じたと考えられた。また，環境宿主側のリスクファクターの違いも関係していると思われる。Picardeau ら[7]の報告では臨床分離菌13株(33.3%) に HIV 感染を認め，そのうち8株がⅡ型に属していた。Taillard ら[6]は，HIV感染が認められる39株 (20.4%) のうち15株がⅡ型であると報告している。また Alcaide ら[4]は彼らの考察の中で，Tortoli ら[25]が検討した69株のうち HIV 感染を認めた株は20株 (29.0%) 含まれ，そのうちのアキュプローブ法で陰性を示した12株がおそらくⅡ型に相当すると述べている。そこで Taillard ら[6]や，Chimara ら[16]は宿主の免疫状態がⅠ型以外の型の感染による *M. kansasii* 症と関連していると考察している。したがって，今回の HIV 感染陰性の *M. kansasii* 症患者由来菌株を対象とした検討から，全身性の重篤な免疫不全をもたない患者群での *M. kansasii* 症はⅠ型が大部分を占めるであろう可能性を支持した。

Tortoli の論説[26]でⅠ型はヒトから，Ⅱ型はヒトもしくは環境から，Ⅲ型からⅤ型は環境から多く分離されるため，Ⅲ～Ⅴ型が分離された場合は colonization の可能性があるとしているが，その後新たに報告されたⅥ型，Ⅶ型に関してはその臨床的意義は未だ不明である。今回われわれが分離したⅥ型による *M. kansasii* 症患者は日本結核病学会の診断基準[8]を満たしていることから colonization の可能性は低いと考えられる。Ⅵ型についての報告例が限られており，今後のデータ蓄積が必要ではあるが，今回のわれわれの結果はⅥ型のヒトへの感染は臨床的に意義があることを強く示唆するものである。

Alcaide ら[4]は *M. kansasii* の *hsp*65-PRA によって得られた5つの型が ITS シークエンスによって塩基上に相違を認めると報告している。今回174株中173株の *hsp*65-PRA と ITS シークエンスの型は一致したが，1株のみが *hsp*65-PRA でⅡb型，ITS シークエンスでⅡ型を示した。これは Iwamoto and Saito[14]の定義するⅠ型とⅡ型の中間型 (atypical type Ⅱ) であり，Ⅱ型からⅠ型への分化を示唆する株の存在が今回の解析においても認められたのは興味深い。

IS*1652*-RFLP の結果，各型間で多型性が認められた。Yang ら[12]は1から11本のバンド間で多型性を示したとしている。また Picardeau ら[7]はⅡ型とⅢ型に IS*1652* 配列は存在するが，Ⅰ型，Ⅳ型，Ⅴ型には存在しなかったとしている。しかし今回の検討でⅡ型以外のⅠ型，Ⅱb型，Ⅵ型の各型にも IS*1652* 配列の存在が認められた。Ⅳ型，Ⅴ型，Ⅶ型の菌株が分離，同定されなかったため，すべての型に IS*1652* 配列が存在するかどうかは現時点では不明だが，今後さらに菌株を蓄積してゆけば，この点は解明されるものと考えられた。

MPTR-RFLP で Ross ら[27]は DNA プローブの pMK1-9 に陽性の *M. kansasii* は共通したバンドパターンを有するが，陰性の *M. kansasii* は不均質であると報告している。しかし Arend ら[28]は22株の *M. kansasii* を対象として ITS シークエンスをターゲットとしたキットである INNO-LiPA Mycobacteria DNA probe test (Innogenetics) で分類したうえで MPTR-RFLP を行った結果，3つに分類されたグループごとに各々の共通するパターンが存在したが，すべての株に疫学的関連性は認められなかったとしている。今回の検討でも IS*1652*-RFLP と同様に各型間の多型性が認められたが，174株由来の患者の居住地域や職場環境といった生活圏は分散しており，疫学的関連性は乏しいと考えられた。

PFGE では Picardeau ら[7]が制限酵素 *Dra* Ⅰ を用いた PFGE パターンから大きなクラスターを形成したグループをパターンⅠと定義し，そのパターンⅠは *hsp*65-PRA でⅠ型に相当したと報告している。またパターンⅠの中に4つの亜分類を認め，そのうち最も多く見られるパターンはⅠaであるとしている。Zhang ら[29]によると，彼らが得たパターン Da (制限酵素 *Dra* Ⅰ処理) と，Iinuma ら[11]が認めた M型 (制限酵素 *Vsp* Ⅰ処理) は上記のパターンⅠaと共通するパターンを有したとしている。そして Zhang ら[29]は供試した71株中，パターン Da の31株と1～3のバンドの違いをもつ33株，それに4～6のバンドの違いをもつ4株の合計68株 (95.8%) にクローナリティーを認めたと報告し，また *hsp*65-PRA で81株中78株 (96.3%) はⅠ型であったとしている。今回われわれの得たグループA (159株) は，目視比較により Zhang らの Da (Iinuma らの M型) に属するものと判断でき，Ⅰ型の中でも特にクローナリティーの高いグループと考えられた。また今回の結果は1施設のみで得られた臨床検体を対象としたものであるが，全国規模の検体を対象とした Iinuma ら[11]の結果と同様に PFGE により他の手法では識別できなかったⅠ型の一部を亜分類できた。したがって，今回の検討からわが国における *M. kansasii* の感染状況を知るうえで重要な知見が得られたと考えられ，同時に今回検討した各種遺伝子型別解析法の中では PFGE が最も分離能の高い手法であることが示唆された (Table 2)。

われわれは，これまでの報告から NTM に対する有用性が認められている各種遺伝子型別解析法を用いて，*M. kansasii* 症例の多い当センター周辺地域で集められた菌株の遺伝子型別特徴の解明を試みたが，大部分はⅠ型の遺伝子型に属しており，全国規模で集積された菌株との間に明確な違いを認めることができなかった。これらの高い分離能をもつ手法を用いても臨床分離株の大部分

Table 2 Comparison of results for *Mycobacterium kansasii* subspecies by different molecular typing methods

Isolate no.	*hsp*65-PRA	Sequencing	PFGE	RFLP***	
		ITS		IS*1652*	MPTR
1043	Ⅵ	type Ⅵ	B pattern	6	vi
962	Ⅰ	type Ⅰ	B	1	i
1098	Ⅰ	type Ⅰ	B	1	i
673	Ⅰ	type Ⅰ	C pattern	1	i
784	Ⅰ	type Ⅰ	C	1	i
737	Ⅰ	type Ⅰ	C	1	i
458	Ⅰ	type Ⅰ	C	1	i
459	Ⅰ	type Ⅰ	C	1	i
1064	Ⅰ	type Ⅰ	C	1	i
492	Ⅰ	type Ⅰ	C	1	i
90	Ⅰ	type Ⅰ	C	1	i
723	Ⅰ	type Ⅰ	C	1	i
o-650	Ⅱ	type Ⅱ	C	2	ii
812*	Ⅱb	type Ⅱ	C	2	ii
780	Ⅱ	type Ⅱ	C	2	ii
Others**	Ⅰ	type Ⅰ	A pattern	1	i

*Atypical type Ⅱ by *hsp*65 sequence
**159 *Mycobacterium kansasii* isolates except for types that were defined on the basis of B, C patterns by PFGE.
***Classification of both RFLPs is based on each homogeneous cluster.

がⅠ型に分類されたことから，*M. kansasii* Ⅰ型は系統発生学的には比較的新しく分化した遺伝子型であると考えられた。したがって，その菌株間でのクローナリティーは高く維持されており，現在までに報告されている *M. kansasii* の遺伝子型別解析手法では同一クローン由来株の判別には限界があるものと思われる。*M. kansasii* の感染様式をより詳細に解明するためには，さらに高い解像度をもつ新たな手法を用いたアプローチが必要であろう。

一方，*M. kansasii* の感染様式の疫学的解明のためには，患者背景からの要因解明も重要である。発症の誘因としてMarrasら[17]は粉塵曝露歴の関与を強く示唆する報告をしており，Alcaideら[30]はホームレスとの関連性を指摘している。よって，鉄工や造船関係の工場が多い当センター周辺の住環境の影響が菌の発症に大きく関係している可能性があると考えられた。また宿主側のリスクとして，HIV陽性患者や，AIDSではないが免疫抑制状態にある患者（腎移植や，長期ステロイド使用）が *M. kansasii* に感染している事例が多く報告されている[31)32)]。今回得られた遺伝子型別のデータを基にしてHIV感染以外の患者背景を加えた詳細なデータベース構築を現在検討中である。

ま と め

今回各種遺伝子型別法を応用して *M. kansasii* の分子疫学的解明を検討した結果，地域特性の解明には至らなかったが，Ⅰ型の蔓延した感染状況が推測された。IS*1652*-RFLPではⅡ型，Ⅲ型以外の型（Ⅰ型，Ⅱb型，Ⅵ型）にIS*1652*配列の存在が見出された。またPFGEにより，Ⅰ型はクローナリティーの高い菌株で形成されていること，およびいくつかの亜分類の存在が示唆された。今後 *M. kansasii* のさらなる疫学的解明のために，より詳細な検討を行う必要があるものと思われた。

文 献

1) The Mycobacteriosis Research Group of the Japanese National Chest Hospitals: Rapid increase of the incidence of lung disease due to *Mycobacterium kansasii* in Japan. Chest. 1983 ; 83 : 890–892.
2) Yang M, Ross BC, Dwyer B: Isolation of a DNA probe for identification of *Mycobacterium kansasii*, including the genetic subgroup. J Clin Microbiol. 1993 ; 31 : 2769–2772.
3) Huang ZH, Ross BC, Dwyer B: Identification of *Mycobacterium kansasii* by DNA hybridization. J Clin Microbiol. 1991 ; 29 : 2125–2129.
4) Alcaide F, Richter I, Bernasconi C, et al.: Heterogeneity and clonality among isolates of *Mycobacterium kansasii*: implications for epidemiological and pathogenicity studies. J Clin Microbiol. 1997 ; 35 : 1959–1964.
5) Devallois A, Goh KS, Rastogi N: Rapid identification of Mycobacteria to species level by PCR-restriction fragment length polymorphism analysis of the *hsp*65 gene and proposition of an algorithm to differentiate 34 Mycobacterial species. J Clin Microbiol. 1997 ; 35 : 2969–2973.

6) Taillard C, Greub G, Weber R, et al.: Clinical implications of *Mycobacterium kansasii* species heterogeneity: Swiss national survey. J Clin Microbiol. 2003 ; 41 : 1240–1244.
7) Picardeau M, Prod'Hom G, Raskine L, et al.: Genotypic characterization of five subspecies of *Mycobacterium kansasii*. J Clin Microbiol. 1997 ; 35 : 25–32.
8) 日本結核病学会非定型抗酸菌症対策委員会：肺非結核性抗酸菌症診断に関する見解—2003年. 結核. 2003 ; 78 : 569–572.
9) Telenti A, Marchesi F, Balz M, et al.: Rapid identification of mycobacteria to the species level by polymerase chain reaction and restriction enzyme analysis. J Clin Microbiol. 1993 ; 31 : 175–178.
10) Richter E, Niemann S, Rüsch-Gerdes S, et al.: Identification of *Mycobacterium kansasii* by using a DNA probe (AccuProbe) and molecular techniques. J Clin Microbiol. 1999 ; 37 : 964–970.
11) Iinuma Y, Ichiyama S, Hasegawa Y, et al.: Large-restriction-fragment analysis of *Mycobacterium kansasii* genomic DNAs and its application in molecular typing. J Clin Microbiol. 1997 ; 35 : 596–599.
12) Yang M, Ross BC, Dwyer B: Identification of an insertion sequence-like element in a subspecies of *Mycobacterium kansasii*. J Clin Microbiol. 1993 ; 31 : 2074–2079.
13) Hermans PWM, van Soolingen D, van Embden JDA: Characterization of a major polymorphic tandem repeat in *Mycobacterium tuberculosis* and its potential use in the epidemiology of *Mycobacterium kansasii* and *Mycobacterium gordonae*. J Bacteriol. 1992 ; 174 : 4157–4165.
14) Iwamoto T, Saito H: Comparative study of two typing methods, *hsp*65 PRA and ITS sequencing, revealed a possible evolutionary link between *Mycobacterium kansasii* typ I and II isolates. FEMS Microbiol Lett. 2006 ; 254 : 129–133.
15) Tenover FC, Arbeit RD, Goering RV, et al.: Interpreting chromosomal DNA restriction patterns produced by pulsed-field gel electrophoresis: criteria for bacterial strain typing. J Clin Microbiol. 1995 ; 33 : 2233–2239.
16) Chimara E, Giampaglia CMS, Martins MC, et al.: Molecular characterization of *Mycobacterium kansasii* isolates in the state of Sãn Paulo between 1995–1998. Mem Inst Oswaldo Cruz. 2004 ; 99 : 739–743.
17) Marras TK, Daley CL: Epidemiology of human pulmonary infection with nontuberculous mycobacteria. Clin Chest Med. 2002 ; 23 : 553–567.
18) Kubín M, Svandová E, Medek B, et al.: *Mycobacterium kansasii* infection in an endemic area of Czechoslovakia. Tubercle. 1980 ; 61 : 107–112.
19) Corbett EL, Blumberg L, Churchyard GJ, et al.: Nontuberculous mycobacteria: defining disease in a prospective cohort of South African miners. Am J Respir Crit Care Med. 1999 ; 160 : 15–21.
20) Dawson DJ, Reznikov M, Blacklock ZM, et al.: Atypical mycobacteria isolated from clinical material in south-eastern Queensland. Pathology. 1974 ; 6 : 153–160.
21) American Thoracic Society: Diagnosis and treatment of disease caused by nontuberculous mycobacteria. Am J Respir Crit Care Med. 1997 ; 156 : S1–S25.
22) Good RC, Snider DE Jr: Isolation of nontuberculous mycobacteria in the United States 1980. J Infect Dis. 1982 ; 146 : 829–833.
23) Horsburgh CR Jr, Selik RM: The epidemiology of disseminated nontuberculous mycobacterial infection in the acquired immunodeficiency syndrome (AIDS). Am Rev Respir Dis. 1989 ; 139 : 4–7.
24) Bloch KC, Zwerling L, Pletcher MJ, et al.: Incidence and clinical implications of isolation of *Mycobacterium kansasii*: results of a 5-year, population-based study. Ann Intern Med. 1998 ; 129 : 698–704.
25) Tortoli E, Simonetti MT, Lacchini C, et al.: Tentative evidence of AIDS-associated biotype of *Mycobacterium kansasii*. J Clin Microbiol. 1994 ; 32 : 1779–1782.
26) Tortoli E: *Mycobacterium kansasii*, species or complex? biomolecular and epidemiological insights. Kekkaku. 2003 ; 78 : 705–709.
27) Ross BC, Jackson K, Yang M, et al.: Identification of a genetically district subspecies of *Mycobacterium kansasii*. J Clin Microbiol. 1992 ; 30 : 2930–2933.
28) Arend SM, Cerdá de Palou E, de Haas P, et al.: Pneumonia caused by *Mycobacterium kansasii* in a series of patients without recognised immune defect. Clin Microbiol Infect. 2004 ; 10 : 738–748.
29) Zhang Y, Mann LB, Wilson RW, et al.: Molecular analysis of *Mycobacterium kansasii* isolates from the United States. J Clin Microbiol. 2004 ; 42 : 119–125.
30) Alcaide F, Benítez MA, Martin R: Epidemiology of *Mycobacterium kansasii*. Ann Intern Med. 1999 ; 131 : 310–311.
31) Witzig RS, Fazal BA, Mera RM, et al.: Clinical manifestations and implications of coinfection with *Mycobacterium kansasii* and human immunodeficiency virus type 1. Clin Infect Dis. 1995 ; 21 : 77–85.
32) Lichtenstein IH, MacGregor RR: Mycobacterial infections in renal transplant recipients: report of five cases and review of the literature. Rev Infect Dis. 1983 ; 5 : 216–226.

Original Article

MOLECULAR EPIDEMIOLOGICAL ANALYSIS OF *MYCOBACTERIUM KANSASII* ISOLATES

[1]Shiomi YOSHIDA, [1]Katsuhiro SUZUKI, [1]Kazunari TSUYUGUCHI, [3]Tomotada IWAMOTO, [1]Masaji OKADA, and [2]Mitsunori SAKATANI

Abstract [Purpose] To make molecular epidemiological analysis of *Mycobacterium kansasii* (*M. kansasii*) isolates.

[Methods] We examined 174 *M. kansasii* isolates from clinical samples of patients at National Hospital Organization Kinki-chuo Chest Medical Center from June 1, 2002 to August 31, 2005 by polymerase chain reaction (PCR) -restriction analysis (PRA) of the heat shock protein (*hsp*) 65 gene (*hsp*65-PRA), sequencing (ITS, 16S-23S internal transcribed spacer, and *hsp*65 for discrepant case between *hsp*65-PRA and ITS sequence), pulsed-field gel electrophoresis (PFGE), and restriction fragment length polymorphism (RFLP) with the major polymorphic tandem repeat (MPTR) probe and the IS*1652* probe of genomic DNA.

[Results] Of the 174 *M. kansasii* isolates, 170 strains were classified as *M. kansasii* type Ⅰ using *hsp*65-PRA, while two isolates belonged to type Ⅱ and one each isolate to type Ⅱb and Ⅵ, respectively. Although the ITS sequence of these isolates also identified the same region of polymorphism by *hsp*65-PRA, only type Ⅱb might be revealed atypical type Ⅱ, a transitional type from typical type Ⅱ to intermediate type Ⅰ by *hsp*65 sequence. The polymorphic patterns by RFLPs with MPTR and IS*1652* probe were shown specific for each homogeneous cluster by *hsp*65-PRA. In addition, 159 isolates were recognized the same common pattern A by PFGE analysis. In contrast, the rest 15 isolates revealed significant polymorphism within 11 isolates of type Ⅰ, and 4 isolates among type Ⅱ, Ⅱb, and Ⅵ.

[Discussion] We verified the *M. kansasii* genotype Ⅰ was predominant, with the same pattern of major worldwide type regions, and reflected a very tight clonal structure. Type Ⅰ was furthermore indicated recognition of subtypes by PFGE analysis.

Key words: *Mycobacterium kansasii*, *hsp*65-PRA, 16S-23S ITS sequencing, PFGE analysis, RFLP analysis

[1]Clinical Research Center, [2]Department of Respiratory Medicine, National Hospital Organization Kinki-chuo Chest Medical Center, [3]Kobe Institute of Health

Correspondence to: Shiomi Yoshida, Clinical Research Center, National Hospital Organization Kinki-chuo Chest Medical Center, 1180 Nagasone-cho, Kita-ku, Sakai-shi, Osaka 591–8555 Japan. (E-mail: dustin@kch.hosp.go.jp)